FULL PAPER

Complementary Absorbing Star-Shaped Small Molecules for the Preparation of Ternary Cascade Energy Structures in Organic Photovoltaic Cells

Hyojung Cha, Dae Sung Chung, Suk Young Bae, Min-Jung Lee, Tae Kyu An, Jihun Hwang, Kyung Hwan Kim, Yun-Hi Kim, Dong Hoon Choi,* and Chan Eon Park**

Two anthracene-based star-shaped conjugated small molecules, 5′,5″-(9,10-bis((4-hexylphenyl)ethynyl)anthracene-2,6-diyl)bis(5-hexyl-2,2′-bithiophene), HBantHBT, and 5′,5″-(9,10-bis(phenylethynyl) anthracene-2,6-diyl)bis(5-hexyl-2,2′-bithiophene), BantHBT, are used as electron-cascade donor materials by incorporating them into organic photovoltaic cells prepared using a poly((5,5-E-alpha-((2-thienyl) methylene)-2-thiopheneacetonitrile)-alt-2,6-[(1,5-didecyloxy)naphthalene])) (PBTADN):[6,6]-phenyl-C71-butyric acid methyl ester ($PC_{71}BM$) blend. The small molecules penetrate the PBTADN:$PC_{71}BM$ blend layer to yield complementary absorption spectra through appropriate energy level alignment and optimal domain sizes for charge carrier transfer. A high short-circuit current (J_{SC}) and fill factor (FF) are obtained using solar cells prepared with the ternary blend. The highest photovoltaic performance of the PBTADN:BantHBT:$PC_{71}BM$ blend solar cells is characterized by a J_{SC} of 11.0 mA cm^{-2}, an open circuit voltage (V_{OC}) of 0.91 V, a FF of 56.4%, and a power conversion efficiency (PCE) of 5.6% under AM1.5G illumination (with a high intensity of 100 mW^{-2}). The effects of the small molecules on the ternary blend are investigated by comparison with the traditional poly(3-hexylthiophene) (P3HT):[6,6]-phenyl-C61-butyric acid methyl ester ($PC_{61}BM$) system.

1. Introduction

Organic semiconductors have recently received considerable attention for their use as active layers in organic photovoltaic cells (OPVs). Organic semiconductors are low-cost, light-weight, and flexible for use in solution-processed photovoltaic devices.[1–4] OPVs prepared with P3HT as the donor and $PC_{61}BM$ as the acceptor have been investigated for use in high-performance photovoltaic devices over the past several years.[4–8] P3HT displays a high carrier mobility of 0.1 cm^2 V^{-1} s^{-1} in organic field-effect transistors (OFETs), largely because it self-organizes into a microcrystalline structure that efficiently transports charge carriers.[4–8] The UV-visible absorption spectrum of P3HT can be red-shifted by thermal annealing to produce nanometer-scale polymer crystalline domains that help transport and collect the separated charge carriers at each electrode.[4–8] The $PC_{61}BM$ acceptor material has been extensively used because it is soluble in common solvents (especially when compared with the solubility of another acceptor material, C_{60}) and it yields appropriate domain sizes in polymer blends.[4–8] Recently, Kim et al. reported a high photon conversion efficiency (PCE) of 5.1% using P3HT:$PC_{61}BM$-based OPVs with a TiO_X optical spacer between the active layer and the cathode.[9]

Despite the enhanced performance of P3HT:$PC_{61}BM$ blend solar cells, P3HT is limited in its utility for solution-processed OPV applications. The uniformity of the domain sizes at high thermal annealing temperatures is difficult to control, and the distribution of domain sizes complicates device optimization.[8–11] The UV-visible absorption range of P3HT displays inefficient overlap with the solar spectrum; P3HT absorbs up to a maximum of 600 nm, regardless of the annealing temperature, thereby missing a significant cross-section of the full solar radiation spectrum. P3HT:$PC_{61}BM$ blend solar cells also produce unnecessary dissociation energy loss due to the large difference between the lowest unoccupied molecular orbital (LUMO) levels of P3HT and $PC_{61}BM$.[8–11] P3HT features a low highest occupied molecular orbital (HOMO) level that

H. Cha, T. K. An, J. Hwang, Prof. C. E. Park
Polymer Research Institute
Department of Chemical Engineering
Pohang University of Science Technology
Pohang, 790-784, South Korea
E-mail: cep@postech.ac.kr
Prof. D. S. Chung
Department of Chemical Engineering
Dong-A University
Pusan, 604-714, South Korea
S. Y. Bae, K. H. Kim, Prof. D. H. Choi
Department of Chemistry
Research Institute for Natural Science
Korea University
Seoul, 136-701, South Korea
E-mail: dhchoi8803@korea.ac.kr
M.-J. Lee, Prof. Y.-H. Kim
Department of Chemistry
Gyeongsang National University
Jinju, 660–701, South Korea
E-mail: ykim@gnu.ac.kr

DOI: 10.1002/adfm.201201913

produces poor oxidative stability. Collectively, these qualities make P3HT:$PC_{61}BM$ solar cells inappropriate for commercial OPV applications.

The alternative development of donor materials often introduces donor–acceptor units into a repeating unit to increase the electron density and reduce the band gap.[12–18] Another approach to enhancing OPV performance is to produce multistructured tandem cells;[19–23] however, these cells have not displayed better PCEs than single cells. A drawback of tandem solar cells is the complexity of cell fabrication including controlling metal based interlayer, which is in contrast to the attractive simplicity of the single-step solution processing of the active layer in bulk heterojunction (BHJ) solar cells.[24–27] An alternative approach involves preparing ternary blend solar cells consisting of either two polymer donors and a fullerene acceptor, one polymer donor and two acceptors, a polymer donor, a fullerene acceptor, and a small molecule, or a polymer donor with a nanoparticle and a fullerene as acceptor that together provide complementary absorption spectra and fuller coverage of the solar radiation spectrum.[28–34] In this case, the energy band edge offsets of the two donor materials must be matched to the transport charge carrier energy, and the three materials, including the acceptor material, should absorb at different wavelengths.[28] Ternary blend solar cells are called ternary cascade energy structures.[24–41] Polymer-polymer-fullerene ternary blend solar cells have not yet yielded PCEs higher than may be obtained from single conventional polymer-fullerene cells.[35–39] Polymer-polymer blends generally have a strong tendency to undergo enthalpy-driven phase-separation.[35–39] Thus, these attempts frequently result in lateral phase separation with domain sizes in the micrometer regime. The performances of polymer-small molecule-fullerene blended solar cells can, theoretically, be better than the performances of polymer-polymer blend solar cells.[28,40,41] Small molecules can act as steps along an energy cascade to assist charge transfer between the electron-donating conjugated polymers and the electron-accepting fullerene derivatives. In addition to providing a complementary absorption spectrum and an appropriate energy level, conjugated small molecules must show good miscibility with the electron donor and electron acceptor materials in order to control the domain size of the ternary blend for efficient exciton dissociation.

In this study, a naphthalene derivative polymer donor material, PBTADN, and the acceptor material, $PC_{71}BM$, were blended with either of two different anthracene-based star-shaped conjugated small molecules, **HBantHBT** and **BantHBT**, which provided intermediate energy levels to produce a ternary cascade energy structure. The effects of the star-shaped conjugated small molecules and, thus, the resulting cascade structure were examined for a P3HT:$PC_{61}BM$ blend system. The chemical structures of the materials used for the active layer of the OPVs are shown in **Figure 1**. A naphthalene derivative polymer, PBTADN, was previously reported to display a high field-effect mobility of 2.5×10^{-2} cm V^{-1} s^{-1} in an OFET and an ordinary PCE of 2.9% in an OPV.[42] We introduced two different anthracene-based star-shaped molecules, **HBantHBT**, and **BantHBT**, which differed in the number of pendant alkyl chains. We previously reported that these molecules display good crystalline self-organization properties and an ordinary

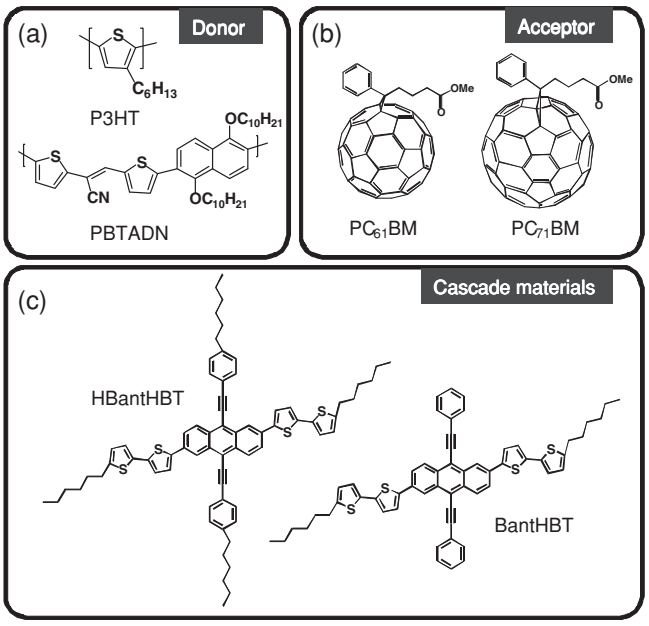

Figure 1. Chemical structures of the molecules used in this study; a) poly(3-hexylthiophene) (P3HT), poly((5,5-E-α-((2-thienyl)methylene)-2-thiopheneacetonitrile)-alt-2,6-[(1,5-didecyloxy)naphthalene])) (PBTADN), b) [6,6]-phenyl-C61-butyric acid methyl ester ($PC_{61}BM$) and [6,6]-phenyl-C71-butyric acid methyl esters ($PC_{71}BM$), and c) 5′,5″-(9,10-bis((4-hexylphenyl)ethynyl)anthracene-2,6-diyl)bis(5-hexyl-2,2′-bithiophene), **HBantHBT**, and 5′,5″-(9,10-bis(phenylethynyl)anthracene-2,6-diyl)bis(5-hexyl-2,2′-bithiophene), **BantHBT**.

field-effect mobility of 5.3×10^{-3} cm V^{-1} s^{-1}.[43] The star-shaped small molecules penetrated the space between polymer chains, thereby controlling the conjugated polymer domain size and improving the charge transport carrier properties by ensuring an appropriate exciton diffusion length (10–20 nm). Recently, a class of antracene-based star-shaped small molecules as an electron donating material has shown high photovoltaic performance in a small molcule:PCBM binary blend system.[44] The small molecules also played an important role as an energetic bridging material to assist in charge carrier transfer from the conjugated polymer to the fullerene derivative. We fabricated ternary cascade solar cells with various blend ratios. The optimal device exhibited an enhanced photocurrent density and FF relative to conventional solar cell devices consisting of a polymer:fullerene binary blend system. Photoluminescence (PL) quenching, external quantum efficiency (EQE), and charge carrier mobility measurements were performed to understand the mechanistic role by which the star-shaped conjugated small molecules improved device performance.

2. Results and Discussion

2.1. Optimal Cell Performance, Achieved by Controlling the Blend Ratio

Optimal solar cell performance is achieved by controlling the blend ratio of each constituent of the ternary blends. In this

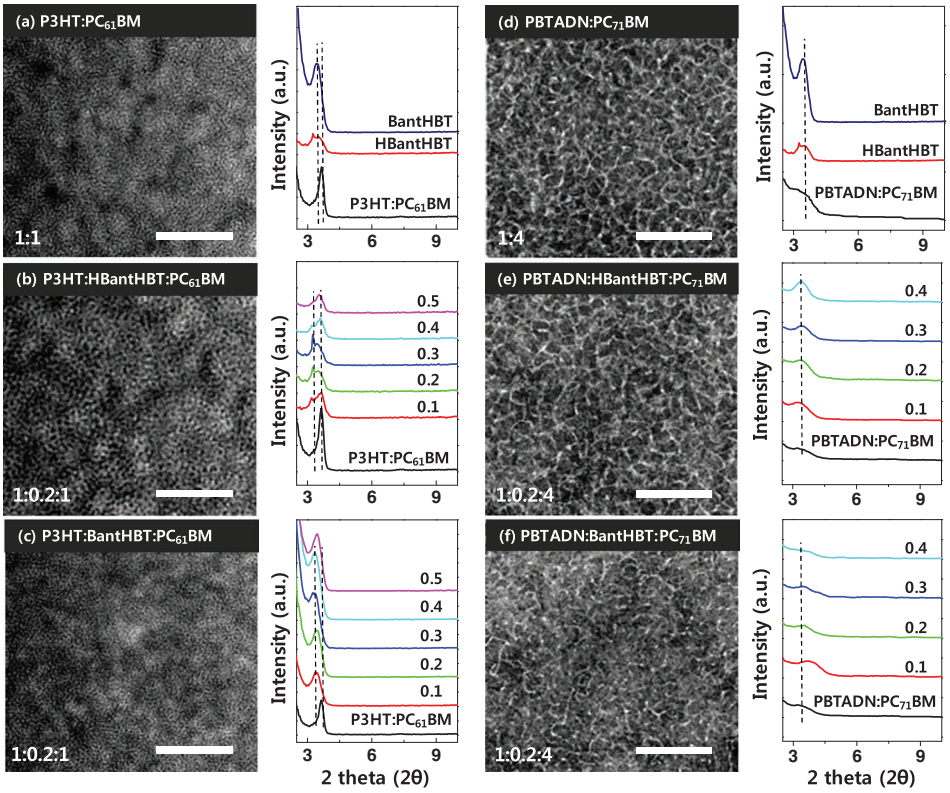

Figure 2. Transmission electron microscopy (TEM) images: a) P3HT:$PC_{61}BM$ (1:1), b) P3HT:**HBantHBT**:$PC_{61}BM$ (1:0.2:1), c) P3HT:**BantHBT**:$PC_{61}BM$ (1:0.2:1), d) PBTADN:$PC_{71}BM$ (1:4), e) PBTADN:**HBantHBT**:$PC_{71}BM$ (1:0.2:4) and f) PBTADN:**BantHBT**:$PC_{71}BM$ (1:0.2:4) with different molecular ratios. Grazing incidence X-ray diffraction scattering data (GIXD) of a) **BantHBT**, **HBantHBT**, P3HT:$PC_{61}BM$ b) P3HT:**HBantHBT**:$PC_{61}BM$, c) P3HT:**BantHBT**:$PC_{61}BM$, d) **BantHBT**, **HBantHBT,** PBTADN:$PC_{71}BM$, e) PBTADN:**HBantHBT**:$PC_{71}BM$ and f) PBTADN:**BantHBT**:$PC_{71}BM$ (Scare bar = 500 nm)

study, the ratio of the star-shaped-small molecules was varied, holding the ratio of electron donor and electron acceptor materials fixed at a previously optimized value.[42,43] The effects of the ternary blend on the morphology, structure, and phase separation were investigated using grazing incidence X-ray diffraction scattering (GIXD), transmission electron microscopy (TEM), and atomic force microscopy (AFM) analysis.

Figure 2 shows representative TEM images of P3HT:star-shaped small molecules:$PC_{61}BM$ films in a 1:0.2:1 blend ratio. The image of the P3HT:$PC_{61}BM$ (1:1) blend cast from chlorobenzene in the absence of star-shaped conjugated small molecules (see Figure 2a) revealed 10–20-nm domains appropriate for charge carrier separation. Blending **HBantHBT** into the P3HT:$PC_{61}BM$ matrix significantly makes the domain size increased to 30–40 nm (see Figure 2b). Figure S1 (Supporting Information) shows TEM images of films formed from various P3HT:star-shaped-small molecule:$PC_{61}BM$ blend ratios, from 1:0.1:1 to 1:0.5:1. The P3HT:**HBantHBT**:$PC_{61}BM$ blends shown in Figure S1a (Supporting Information) reveal that the domain size increased as the ratio of star-shaped-small molecules increased. By contrast, the domains in the P3HT:**BantHBT**:$PC_{61}BM$ blends did not change upon addition of the small molecules (see Figure S1b, Supporting Information). Changes in the vertically layered ordering of the conjugated polymer structures upon the addition of the star-shaped small molecules were examined using GIXD measurements. The GIXD patterns were similar to the linear sum of the GIXD patterns of P3HT:$PC_{61}BM$ and **HBantHBT** (see Figure 2b). The film formed by spin-casting yielded separate P3HT and **HBantHBT** crystalline domains. On the other hand, the P3HT:$PC_{61}BM$ and P3HT:**BantHBT**:$PC_{61}BM$ (1:0.2:1) films showed uniform 10–20-nm domains (see Figure 2c). Interestingly, the inter-lamellar distances among the P3HT polymer along the direction of the side chains increased upon the addition of **BantHBT** small molecules, as confirmed by GIXD (see Figure 2c). In other words, **BantHBT** intercalated into the free spaces between adjacent polymer backbones, inducing a longer inter-lamellar distance.

The interfacial areas between the conjugated polymers and the electron acceptor strongly affected the exciton dissociation yield. Therefore, the optimal polymer domain size facilitated exciton dissociation and the transport of charge carriers in the active layer.[44–48] Because the small molecule **HBantHBT** formed separated crystalline domains apart from those of P3HT, its bigger domain size could have negatively influenced exciton dissociation and charge transport; however, **BantHBT** penetrated the P3HT and $PC_{61}BM$ domains; therefore, the P3HT:**BantHBT**:$PC_{61}BM$ blend films showed a homogeneous morphology and small domains with good miscibility among the three materials, as confirmed by TEM imaging. As a

result, better photovoltaic properties were expected from the P3HT:**BantHBT**:$PC_{61}BM$ blend cells than from the blend films involving **HBantHBT**.

The TEM images of the PBTADN:star-shaped-small molecules:$PC_{71}BM$ blend films are shown in Figure S2 (Supporting Information). After spin-casting, the ternary blend films containing either of the small molecules yielded network blend films with fibril-like structures. Neither blend film (PBTADN:**HBantHBT**:$PC_{71}BM$ or PBTADN:**BantHBT**:$PC_{71}BM$) showed significant morphological changes in the TEM images as the ratio of small molecules was increased from 1:0.1:4 to 1:0.4:4. Figure 2d–f show that increasing the ratio of **HBantHBT** in the PBTADN:$PC_{71}BM$ blend increased the first polymer Bragg reflection peak in the GIXD pattern. On the other hand, the intensity of the first polymer Bragg reflection peak in films containing **BantHBT**, which produced relatively small domains, remained nearly constant over all small molecule ratios tested. These observations agree with the morphological changes in P3HT:$PC_{61}BM$ observed with each of the small molecules, although the degree of change was much less pronounced in the GIXD patterns. The conjugated small molecule, **HBantHBT** could not penetrate into the PBTADN:$PC_{71}BM$ blend; thus, the addition of the molecule merely increased the crystallinity of the polymer. By contrast, **BantHBT** mixed readily with PBTADN and $PC_{71}BM$.

These results were related to the number of alkyl chain substitutions in the small molecules, **HBantHBT** and **BantHBT**.[43,44,48,49] Anthracene-based star-shaped conjugated small molecules with four alkyl chains yielded OFETs with a higher performance than analogous small molecules with two alkyl chains.[43,44,48,49] A comparison of the d-spacings of the two molecules clearly showed that the **HBantHBT** molecules containing four hexyl peripheral moieties exhibited larger d-spacings than the **BantHBT** molecules.[43,44,48,49] The larger lamellar ordering among **HBantHBT** was attributed to the two-dimensional ordering induced by the interactions between the biaxial hexyl peripheral moieties;[43,44,48,49] therefore, **HBantHBT** displayed better molecular ordering than **BantHBT**.

TEM provided information along the vertical direction by detecting electrons projected through the entire film; by contrast, AFM provides information about the surface of an active layer (see Figure S3 and S4, Supporting Information). To further support our argument, we characterized the morphologies of the conjugated polymer:fullerene composite films, prepared using various ratios of the star-shaped small molecules, by AFM. The conditions under which films were prepared for AFM imaging were the same as those used to prepare films for the other experiments, for comparison purposes. Figure S3 and S4 (Supporting Information) show the typical height images of the blend films processed with different ratios of small molecules (the image size is 5 μm × 5 μm). The P3HT:$PC_{61}BM$ or PBTADN:$PC_{71}BM$ films blended with **HBantHBT** revealed a top surface roughness that increased dramatically with widespread phase separation. By contrast, the films containing **BantHBT** molecules exhibited homogeneous morphologies. Evidently, blending **BantHBT** into the P3HT:$PC_{61}BM$ or PBTADN:$PC_{71}BM$ matrix did not significantly modify the surface topography. These results were consistent with the good miscibility and low phase separation observed for the conjugated polymer and **BantHBT**.

The photovoltaic properties of the conjugated polymers mixed with the star-shaped conjugated small molecules were investigated in BHJ solar cells using the following configuration; glass/indium tin oxide (ITO)/poly(3,4-ethylenedioxythiophene):poly(styrenesulfonate)(PEDOT:PSS)/active layer/LiF/Al. The ratio of the conjugated polymer:fullerene derivative was optimized at 1:1 (w/w) for P3HT:$PC_{61}BM$ in chlorobenzene (CB), and 1:4 (w/w) for PBTADN:$PC_{71}BM$ dichlorobenzene (DCB), as described previously.[42,43] Photovoltaic devices were tested under AM 1.5G illumination at 100 mW cm^{-2}, and the active areas of the devices were 0.09 cm^2. All devices had similar layer thicknesses on the order of 120 nm for the P3HT:$PC_{61}BM$ layer and 50 nm for the PBTADN:$PC_{71}BM$ layer, as determined using the alpha-stepper. Variations in J_{SC} displayed by the ternary blend devices could be attributed mainly to the morphological/structural changes caused by the small molecules.

Figure S5 (Supporting Information) presents the current density–voltage (*J–V*) curves for devices prepared from P3HT:small molecules:$PC_{61}BM$ blends for various ratios of the small molecule. Table S1 (Supporting Information) lists the measured device operating parameters J_{SC}, V_{OC}, FF, and PCE as a function of the small molecule concentration. The values of J_{SC}, FF, and PCE decreased as the concentration of small molecules increased in the P3HT:**HBantHBT**:$PC_{61}BM$ films. The P3HT:**BantHBT**:$PC_{61}BM$ cells showed an optimal performance at a 1:0.2:1 blend ratio, yielding the highest J_{SC} and FF values for rations between 1:0.1:1 and 1:0.5:1.

Figure 3a displays the *J–V* curves for devices prepared using a 1:1 blend ratio of P3HT:$PC_{61}BM$ with star-shaped conjugated small molecules. These layers were fabricated via slow growth using a high boiling point solvent (CB), followed by annealing at 150 °C for 20 min. The conventional P3HT:$PC_{61}BM$ device exhibited a J_{SC} of 8.6 mA cm^{-2}, a V_{OC} value of 0.62 V, and a PCE of 3.0%. The best devices were those cast from solutions containing a 1:0.2:1 ratio of P3HT:**BantHBT**:$PC_{61}BM$. The device cast from a solution containing small amounts of **BantHBT** exhibited high values of J_{SC}, 9.8 mA cm^{-2}, V_{OC}, 0.62 V, and a PCE of 3.7%. The device based on P3HT:**HBantHBT**:$PC_{61}BM$ (1:0.2:1) delivered values of J_{SC} and V_{OC} of 6.6 mA cm^{-2} and 0.62 V, respectively. With a FF of 61.0%, this device gave a PCE of 2.5%.

Figure 3b shows the *J–V* characteristics of PBTADN:$PC_{71}BM$ devices blended with each small molecule. As the concentration of HBantHBT increased, the current densities and FFs increased to 1:0.2:4 ratio of PBTADN:HBantHBT:$PC_{71}BM$ and then both decreased, resulting in an absolute decrease in the efficiency, as shown in Figure S6 and Table S2 (Supporting Information). **Table 1** summarizes the V_{OC}, J_{SC}, FF, and PCE of the PBTADN:small molecule:$PC_{71}BM$ (1:0.2:4)-based devices. A V_{OC} in the range of 0.89–0.91 V was insensitive to the small molecule loading ratio, whereas the J_{SC}, FF, and PCE depended strongly on the small molecule loading ratio. The PBTADN:**BantHBT**:$PC_{71}BM$ film with weight ratio of 1:0.2:4 gave the best performance: the V_{OC}, J_{SC}, FF, and PCE reached 0.91 V, 11.0 mA cm^{-2}, 56.4%, and 5.6%, respectively. In conclusion, the improved J_{SC}, and FF yielded an enhanced PCE of 5.6% and an 87% efficiency enhancement relative to that of the PBTADN:$PC_{71}BM$ device prepared without **BantHBT** (see **Figure 4**).

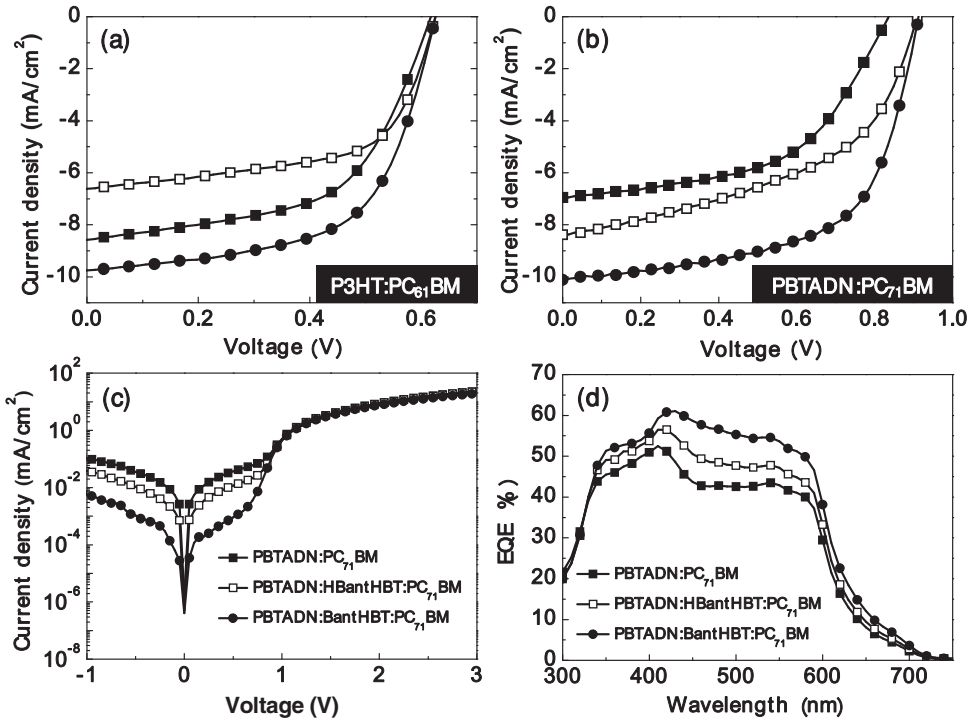

Figure 3. Performance of photovoltaic cells prepared with each small molecule. a) P3HT:$PC_{61}BM$ (1:1) (■), P3HT:**HBantHBT**:$PC_{61}BM$ (1:0.2:1) (□), and P3HT:**BantHBT**:$PC_{61}BM$ (1:0.2:1) (•); b) PBTADN:$PC_{71}BM$ (1:4) (■), PBTADN:**HBantHBT**:$PC_{71}BM$ (1:0.2:4) (□), and PBTADN:**BantHBT**:$PC_{71}BM$ (1:0.2:4) (•). c) Current–voltage (*J*–*V*) curves under dark conditions. d) Incident photon-to-current efficiency (IPCE) for the organic solar cells; PBTADN:$PC_{71}BM$ (1:4) (■), PBTADN:**HBantHBT**:$PC_{71}BM$ (1:0.2:4) (□), and PBTADN:**BantHBT**:$PC_{71}BM$ (1:0.2:4) (•).

Table 1. Photovoltaic cells performance parameters for P3HT:$PC_{61}BM$, P3HT:**HBantHBT**:$PC_{61}BM$, P3HT:**BantHBT**:$PC_{61}BM$, PBTADN:$PC_{71}BM$, PBTADN:**HBantHBT**:$PC_{71}BM$, and PBTADN:**BantHBT**:$PC_{71}BM$.

Device	PCE [%]	V_{OC} [V]	J_{SC} [mA cm $^{-2}$]	FF [%]
P3HT:$PC_{61}BM$	3.0	0.62	8.6	55.8
P3HT:**HBantHBT**:$PC_{61}BM$	2.5	0.62	6.6	61.0
P3HT:**BantHBT**:$PC_{61}BM$	3.7	0.62	9.8	60.4
PBTADN:$PC_{71}BM$	3.0	0.83	6.9	53.1
PBTADN:**HBantHBT**:$PC_{71}BM$	4.1	0.89	8.7	52.1
PBTADN:**BantHBT**:$PC_{71}BM$	5.6	0.91	11.0	56.4

2.2. Electrochemical and Optical Properties (CV, UV, and PL Measurements)

Optical and electrical matching between the conjugated polymer, the star-shaped small molecule, and the fullerene derivative was required for optimization of the ternary blend solar cells. Electrochemical analysis showed that the HOMO energy level of HBantHBT was –5.4 eV and that of BantHBT was –5.7eV. The LUMO level could be determined by the optical band gaps of **HBantHBT** and **BantHBT** (2.1 and 2.1 eV, respectively). **Figure 5**a,b summarize the HOMO and LUMO levels of the P3HT:$PC_{61}BM$ and PBTADN:$PC_{71}BM$ films, respectively, prepared with **HBantHBT** and **BantHBT**, as determined by the electrochemical and optical measurements. The two star-shaped small molecules displayed electronic levels that were properly positioned with respect to the P3HT:$PC_{61}BM$ blend. The HOMO levels were positioned between the HOMO levels of P3HT and $PC_{61}BM$. The LUMO level of **HBantHBT** was higher than the level of PBTADN in the PBTADN:$PC_{71}BM$ blend, which contributed to the poor performance of this blend. Although the difference between the LUMO levels of PBTADN and **BantHBT** was 0.1 eV, the excitons could be separated and collected at each electrode because the difference between the LUMO levels of PBTADN and $PC_{71}BM$ provided a driving force that opposed exciton recombination. The separated charge carriers could diffuse and dissociate due to the built-in potential between the cathode and anode. As a consequence, photo-induced charge transfer was energetically favorable in the blends comprising the conjugated polymer, star-shaped conjugated small molecules, and fullerene derivatives.

As shown in Figure 5c,d, P3HT and PBTADN showed absorption maxima at 523 and 531 nm, respectively. The star-shaped conjugated molecules **HBantHBT** and **BantHBT** showed the same maximum absorption at 388 nm, with complementary absorption spectra in the ternary blend solar cells. As the **HBantHBT** content in the P3HT polymer matrix increased from 0 to 50 wt%, the absorption intensity over the region 500–650 nm changed, as shown in Figure S7a (Supporting Information). Interestingly, the red shoulders at 556 and 605 nm in the P3HT:**HBantHBT**:$PC_{61}BM$ blend layers increased remarkably as the weight ratio of **HBantHBT** increased; however, the red

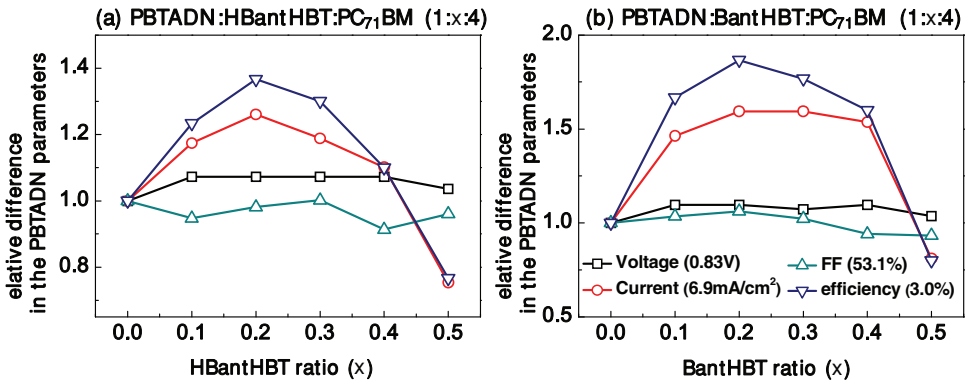

Figure 4. Relative differences in the PBTADN parameters: open circuit voltage (□), current density (○), fill factor (△), and power conversion efficiency (▽) for the a) PBTADN:**HBantHBT**:$PC_{71}BM$ and b) PBTADN:**BantHBT**:$PC_{71}BM$ films prepared with different molecular weight ratios.

shoulders in the P3HT:**BantHBT**:$PC_{61}BM$ blend layers decreased upon the addition of **BantHBT**, as shown in Figure S7b (Supporting Information). Therefore, the P3HT:**HBantHBT**:$PC_{61}BM$ (1:0.2:1) blend layer showed stronger π–π stacking interactions in the ternary blend system than in the P3HT:**BantHBT**:$PC_{61}BM$ blend layer. On the other hand, the P3HT:**BantHBT**:$PC_{61}BM$ cell efficiently absorbed light across the solar radiation spectrum (see **Figure 6**a). By increasing the ratio of **BantHBT** in the PBTADN:$PC_{71}BM$ blend solar cells (Figure S8, Supporting Information), the absorption range became slightly red-shifted by 5 nm and the intensity of the absorption increased, as shown in Figure 6b. The absorption cross-sections of the blend films processed using **HBantHBT** and **BantHBT** did not differ significantly, although the absorption cross-section of the blend film prepared using the small molecules exceeded that of the PBTADN:$PC_{71}BM$ film prepared without the small molecules,

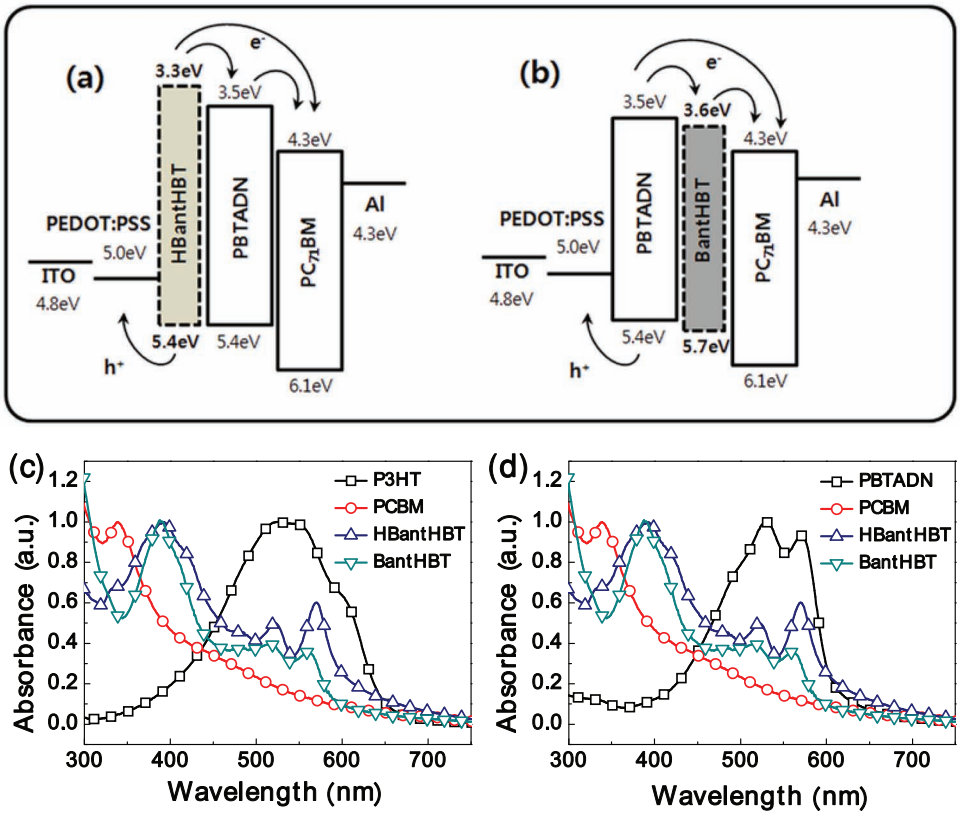

Figure 5. Energy level diagram of the a) P3HT:small molecules:$PC_{61}BM$ and b) PBTADN:small molecules:$PC_{71}BM$ devices. UV-visible absorption spectra of c) P3HT (□), $PC_{61}BM$ (○), **HBantHBT** (△), and **BantHBT** (▽) films, and d) PBTADN (□), $PC_{71}BM$ (○), **HBantHBT** (△), and **BantHBT** (▽) films, respectively.

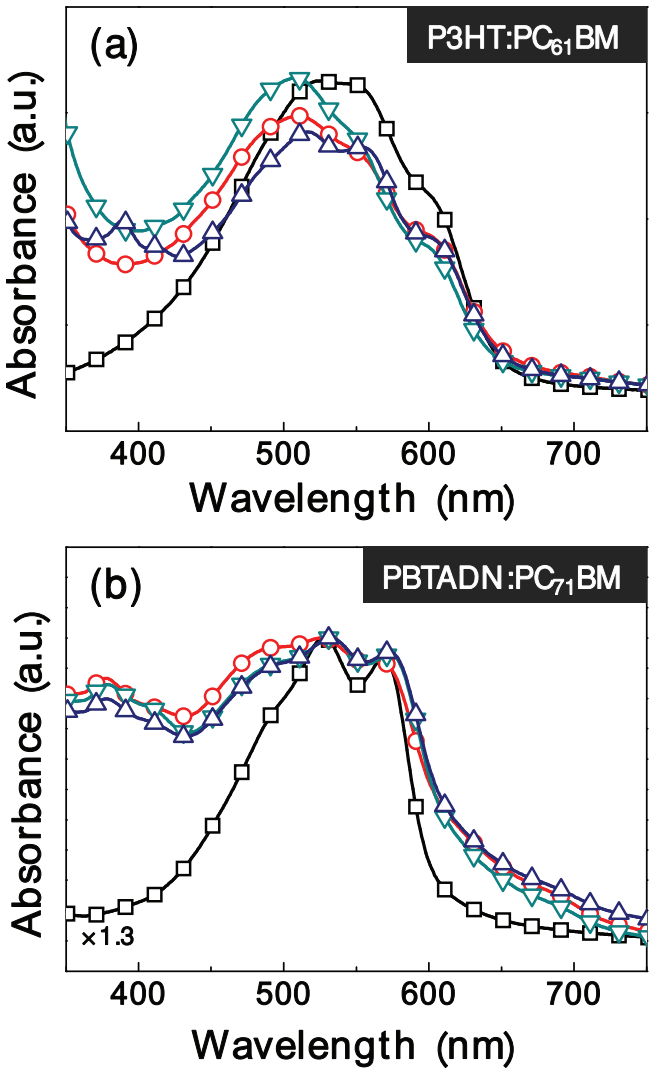

Figure 6. UV-visible absorption spectra of a) P3HT (□), P3HT:$PC_{61}BM$ (○), P3HT:**HBantHBT**:$PC_{61}BM$ (△), and P3HT:**BantHBT**:$PC_{61}BM$ (▽), and b) PBTADN (□), PBTADN:$PC_{71}BM$ (○), PBTADN:**HBantHBT**:$PC_{71}BM$ (△), and PBTADN:**BantHBT**:$PC_{71}BM$ (▽).

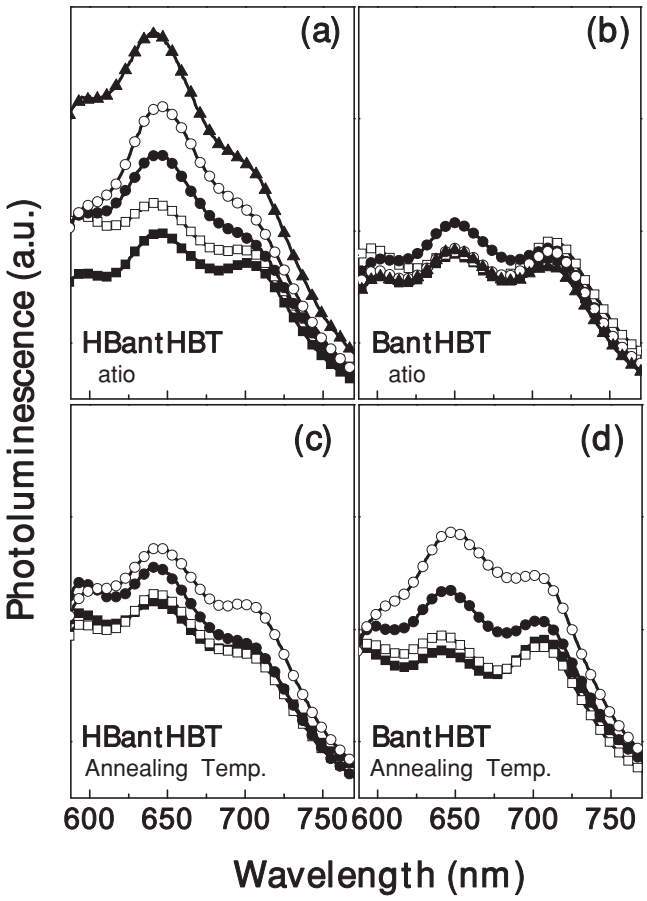

Figure 7. Photoluminescence (PL) spectra of a) PBTADN:**HBantHBT**:$PC_{71}BM$ and b) PBTADN:**BantHBT**:$PC_{71}BM$ thin films with different molecular weight ratios; 1:0:4 (■), 1:0.1:4(□), 1:0.2:4 (•), 1:0.3:4 (○) and 1:0.4:4 (▲), and c) PBTADN:**HBantHBT**:$PC_{71}BM$ and d) PBTADN:**BantHBT**:$PC_{71}BM$, annealed at various temperatures: as-cast (■), 80 °C (□), 120 °C (•), and 150 °C (○).

for a given active layer thickness. The addition of small molecules to the PBTADN:$PC_{71}BM$ blend film increased the light absorption intensity and slightly red-shifted the absorption spectrum.

The PL spectra of the PBTADN:$PC_{71}BM$ blend showed remarkable changes in the PL intensity for higher concentrations of the small molecules (see **Figure 7**). The intensity of the PL spectra of the PBTADN:$PC_{71}BM$ layer prepared with **HBantHBT** (Figure 7a) clearly showed that the presence of **HBantHBT** increased the PL intensity, suggesting an increase in the nonradiative quenching pathways in the more aggregated materials. The PBTADN:$PC_{71}BM$ layer prepared with **BantHBT** displayed a constant PL intensity, even for a small molecule concentration of 50 wt%, as shown in Figure 7b. The PL spectra revealed that the photogenerated excitons in PBTADN:$PC_{71}BM$ prepared with **BantHBT** dissociated more effectively to yield separated charge carriers. Annealing of the PBTADN:$PC_{71}BM$ films prepared with small molecules slightly increased the PL intensity by reducing the phase separation, as shown in Figure 7c,d.

2.3. Device Performance, Dark Current, EQE, and SCLC

We confirmed that the PBTADN:**BantHBT**:$PC_{71}BM$ (1:0.2:4) blend cell gave the best performance, with values of V_{OC}, J_{SC}, FF, and PCE of 0.91 V, 11.0 mA cm^{-2}, 56.4%, and 5.6%, respectively. To determine whether charge carrier transport in this blend was more efficient than in the PBTADN:**HBantHBT**:$PC_{71}BM$ photovoltaic cells, we measured the *J–V* curves under dark current conditions, the EQE spectra, and the space charge-limited current (SCLC).

Figure 3c shows the *J–V* curves in the dark, in which a low leakage current was observed for the PBTADN:**BantHBT**:$PC_{71}BM$ cell. This indicated that the **BantHBT** small molecules provided more effective charge transport in the BHJ solar cells than in the PBTADN:$PC_{71}BM$ or PBTADN:**HBantHBT**:$PC_{71}BM$ cells.

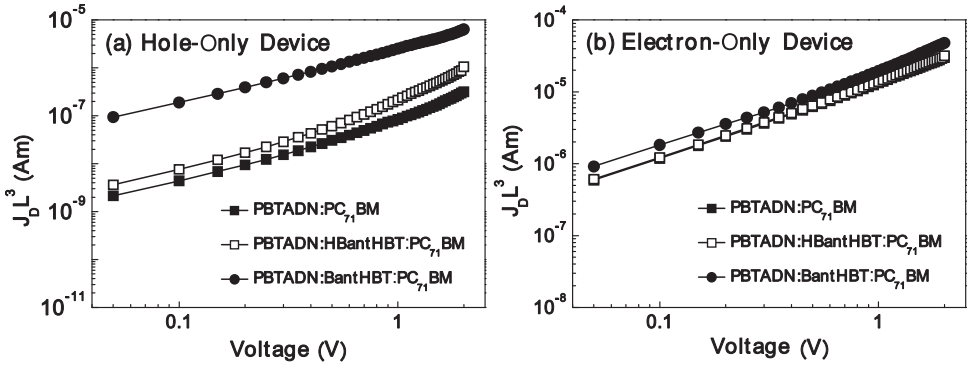

Figure 8. Electron- ($\mu_{e,blend}$) and hole ($\mu_{h,blend}$)-only mobilities of the blends composed of PBTADN:PC_{71}BM (1:4) (■), PBTADN:**HBantHBT**:PC_{71}BM (1:0.2:4) (□), and PBTADN:**BantHBT**:PC_{71}BM (1:0.2:4) (•).

Equation (1) suggests a linear dependence of V_{OC} on the interfacial energy gap (ΔE_{DA}). J_{SO}, in particular, played a role in controlling the V_{OC}.[50,51] The molecular properties that minimized J_{SO} for a given ΔE_{DA} were determined by considering three different cells:[51] PBTADN:PC_{71}BM, PBTADN:**BantHBT**:PC_{71}BM, and PBTADN:**HBantHBT**:PC_{71}BM cells. Despite the similar HOMO energies of 5.4 eV for PBTADN, 5.4 eV for **HBantHBT**, and 5.7 eV for **BantHBT**, the V_{OC} values for the three cells were considerably different: 0.83, 0.89, and 0.91 eV, for PBTADN:PC_{71}BM, PBTADN:**BantHBT**:PC_{71}BM, and PBTADN:**HBantHBT**:PC_{71}BM cells, respectively. The differences in V_{OC} arose from the large differences in the current-dependent terms of Equation (1);[51] that is, J_{SO} was larger in PBTADN:PC_{71}BM than in the other cells.

$$V_{OC} = \frac{nkT}{q} \ln\left(\frac{J_{SC}}{J_{SO}}\right) + \frac{\Delta E_{DA}}{2q} \quad (1)$$

Here, n is the diode ideality factor, k is the Boltzmann constant, T is the Kelvin temperature, and ΔE_{DA} is the interfacial energy gap between the donor and acceptor.[51] The magnitude of J_{SO} depends on several material properties that determine the carrier generation and recombination rate, independent of the energy barrier, ΔE_{DA}.[51]

The EQE spectra for the devices are shown in Figure 3d. The spectra revealed an excellent photocurrent response over the absorption range 300–700 nm. The shapes of the EQE plots for the devices were similar to the corresponding absorption spectra (Figure 6b), indicating that the full polymer absorption range contributed to photocurrent generation. The devices prepared from PBTADN:PC_{71}BM yielded an enhanced EQE over the whole absorption range of 300–700 nm upon the addition of small molecules. The 400–600 nm range, in particular, yielded a remarkable enhancement in EQE. The highest EQE value for the PBTADN:**BantHBT**:PC_{71}BM blend film approached 61% at 430 nm, 16% greater than that for PBTADN:PC_{71}BM (Figure S9, Supporting Information). These results clearly showed that the enhanced EQEs for PBTADN:**HBantHBT**:PC_{71}BM and PBTADN:**BantHBT**:PC_{71}BM were consistent with the improved PCEs in the devices.

Indeed, large differences were observed in the mobility ratios (hole-only mobility (μ_e)/electron-only mobility (μ_h)) of the PBTADN:PC_{71}BM, PBTADN:**HBantHBT**:PC_{71}BM, and PBTADN:**BantHBT**:PC_{71}BM blends (**Figure 8**). In addition, μ_e/μ_hs (**Table 2**) was strongly related to the PCE, as shown in Figure 3b. Table 2 shows that the presence of small amounts of the small molecules in the PBTADN:PC_{71}BM blend films increased J_{SC} remarkably (Table 1), and the μ_e/μ_hs ratio decreased. The small molecules may have influenced the absorption spectra, charge separation, the formation of percolation paths, or an the improved μ_h, all of which would improve the efficiency of the solar cells.

3. Conclusions

We have demonstrated that J_{SC}, V_{OC}, and the FF of a BHJ solar cell based on a conjugated polymer:fullerene blend can be enhanced by the addition of small amounts of a conjugated small molecule, **BantHBT**, which displayed good miscibility with the conjugated polymers, increased the absorption cross-section of the active layer, and balanced the charge carrier mobilities. PL analysis and an enhanced EQE supported the effects of **BantHBT**. Photo-induced charge transfer from the conjugated polymer via small molecules to the fullerene derivatives contributed to the overall photocurrent generation in the cell. The high-performance PBTADN:**BantHBT**:PC_{71}BM blend solar cells exhibited high values of J_{SC} and V_{OC} due to the fine-tuning of the energy levels and the control over domain size, yielding optimal charge carrier transport by incorporating the conjugated small molecule, **BantHBT**, into the PBTADN:PC_{71}BM blend. The PCE of the ternary blend system increased by almost 87%, relative to

Table 2. Hole (μ_h) and electron (μ_e) mobilities of PBTADN:PC_{71}BM (1:4) films incorporated with or without small molecules, **HBantHBT** and **BantHBT**, evaluated using the Mott–Gurney law.

Device	μ_h [cm^2/Vs]	μ_e [cm^2/Vs]	μ_e/μ_h
PBTADN:PC_{71}BM	3.90×10^{-8}	5.77×10^{-6}	147.9
PBTADN:**HBantHBT**:PC_{71}BM	9.37×10^{-8}	5.90×10^{-6}	93.1
PBTADN:**BantHBT**:PC_{71}BM	1.08×10^{-6}	8.53×10^{-6}	7.94

the binary blend without **BantHBT**. In summary, ternary blends provide a simple and effective approach to expanding the overall photoresponse of a BHJ solar cell.

4. Experimental Section

Organic solar cells were fabricated with the structure ITO/PEDOT:PSS/conjugated polymer:star-shaped molecule:$PC_{71}BM$/LiF/Al. A glass substrate with a pre-patterned ITO (active layer of 0.09 mm^2) was ultrasonicated in detergent, deionized water, CMOS-grade acetone, and isopropanol, and the surface of the glass substrate was modified by UV-ozone treatment for 20 min. PEDOT:PSS (Bay P VP AI4083, Bayer AG), for hole injection, was spin-coated at 4000 rpm for 60 s to a thickness of 30–40 nm on the cleaned ITO-patterned glass substrate after filtration through a 0.45-μm filter, followed by baking in an oven at 120 °C for more than an hour.

The organic solar cells consisted of conjugated polymers as electron donors and a fullerene derivative as the electron acceptor. The conjugated polymer, PBTADN, was synthesized via a palladium-catalyzed Suzuki coupling reaction, as described previously.[42] The molecular weight of PBTADN was 44 791 g mol^{-1}. The electron donor conjugated polymer, P3HT, was obtained from Rieke Metal. The anthracene-based star-shaped molecules, **HBantHBT** and **BantHBT**, were synthesized via a Pd-catalyzed Sonogashira coupling reaction. The $PC_{61}BM$ and $PC_{71}BM$ fullerene derivative the electron acceptors (99.5%) were obtained from NanoC. Solutions with various concentration ratios of the star-shaped molecule relative to the conjugated polymer:fullerene derivative were prepared in dichlorobenzene to yield 20 mg/mL solutions that were stirred in a glove box under a nitrogen atmosphere overnight. The blended solutions were spin-coated at 1000 rpm for 60 s to a thickness of 100 nm on top of the PEDOT:PSS layer, then annealed at various temperatures for 20 min on a hot plate in the glove box. The LiF and Al cathodes were thermally deposited to thicknesses of 1 and 100 nm, respectively, onto the surface of the active layer.

The *J–V* characteristics were measured using a Keithley 4200 source measurement unit, in the dark and under AM 1.5G solar illumination (Oriel 1 kW solar simulator) with respect to a reference cell PVM 132 calibrated at the National Renewable Energy Laboratory at an intensity of 100 mW cm^{-2}. The EQE was performed using a photomodulation spectroscopic setup (model Merlin, Oriel), a calibrated Si UV detector, and an SR570 low noise current amplifier. UV-visible (Cary:Varian Co.) and PL (FR 650, JASCO Co.) measurements were used to analyze the optical properties of the conjugated polymer:fullerene blend layers. The AFM (Multimode IIIa, Digital Instruments) was operated in tapping mode to acquire images of the surfaces of the conjugated polymer:fullerene derivative blend layers. For TEM measurements, the conjugated polymer:fullerene derivative layers on a water-soluble PEDOT:PSS substrate were floated on the surface of deionized water and picked up using 200-mesh copper TEM grids. TEM images were obtained using a HITACHI-7600 operated at 100 kV.

Hole-only polymer devices were fabricated on top of a pre-patterned ITO substrate. After cleaning the ITO with aqueous detergent, deionized water, acetone, and 2-propanol, UV-ozone treatment was applied for 15 min. PEDOT:PSS (Baytron P TP AI 4083, Bayer AG) was spin-coated from an aqueous dispersion phase to a layer 36-nm thick. The coated substrate was then baked at 120 °C for 60 min. After baking, a solution of the copolymer in chloroform was spin-cast on top of the PEDOT:PSS layer to a thickness of 50 nm, and the samples were dried for 6 h at room temperature under vacuum conditions. The Pd electrode was deposited by thermal evaporation under a vacuum of $\approx 10^{-6}$ Torr. A similar approach was employed to measure the hole-only mobility of the polymer:$PC_{71}BM$ blend using the SCLC method with a device structure of ITO/PEDOT:PSS/polymer:$PC_{71}BM$/Au. Electron-only devices (Al/polymer:PCBM/Al) were fabricated, and their *J–V* characteristics were investigated in the dark. The SCLC mobilities were estimated using the Mott–Gurney square law,[52]

$$J = \frac{9}{8}\varepsilon_0\varepsilon_r\mu_h\frac{V^2}{L^3}$$

where J is the current density, L is the film thickness of the active layer, μ_h is the hole mobility, ε_r is the relative dielectric constant of the transport medium, ε_0 is the permittivity of free space (8.85×10^{-12} F m^{-1}), V is the internal voltage in the device and $V = V_{appl} - V_r - V_{bi}$, V_{appl} is the voltage applied to the device, V_r is the voltage drop due to the contact resistance and series resistance across the electrodes, and V_{bi} is the built-in voltage due to the relative work function difference between the two electrodes. V_{bi} can be determined from the transition between the Ohmic region and the SCLC region.

Supporting Information

Supporting Information is available from the Wiley Online Library or from the author.

Acknowledgements

This work was supported by Pohang Accelerator Laboratory (PAL) and a grant (2011-0031639) from the Center for Advanced Soft Electronics under the Global Frontier Research Program of the Ministry of Education, Science and Technology, Korea. This work was also supported by a grant from the Korea Science and Engineering Foundation (KOSEF), funded by the Korean Government (MEST) (2012-0000127) and (2011-000310).

Received: July 10, 2012
Revised: September 10, 2012
Published online: October 23, 2012

[1] R. F. Service, *Science* **2011**, *332*, 293.
[2] M. A. Green, K. Emery, Y. Hishikawa, W. Warta, *Prog. Photovoltaics* **2011**, *19*, 84.
[3] A. Facchetti, *Chem. Mater.* **2011**, *23*, 733.
[4] P.-L. T. Boudreault, A. Najari, M. Leclerc. *Chem. Mater.* **2011**, *23*, 456.
[5] F. Padinger, R. S. Rittberger, N. S. Sariciftci, *Adv. Funct. Mater.* **2003**, *13*, 85.
[6] W. Ma, C. Yang, X. Gong, K. Lee, A. J. Heeger, *Adv. Funct. Mater.* **2005**, *15*, 1617.
[7] G. Li, V. Srotriya, J. Huang, Y. Yao, T. Moriarty, K. Emery, Y. Yang, *Nat. Mater.* **2005**, *4*, 864.
[8] C. J. Ko, J. K. Lin, F. C. Chen, *Adv. Mater.* **2007**, *19*, 3520.
[9] J. Y. Kim, S. H. Kim, H.-H. Lee, K. Lee, W. Ma, X. Gong, A. J. Heeger, *Adv. Mater.* **2006**, *18*, 572.
[10] T. Erb, U. Zhokhavets, G. Gobsch, S. Raleva, B. Stuhn, P. Schilinsky, C. Waldauf, C. J. Brabec, *Adv. Funct. Mater.* **2005**, *15*, 1193.
[11] L. J. A. Koster, V. D. Mihailetchi, P. W. M. Blom, *Appl. Phys. Lett.* **2006**, *88*, 093511.
[12] L. Dou, J. Gao, E. Richard, J. You, C.-C. Chen, K. C. Cha, Y. He, G. Li, Y. Yang. *J. Am. Chem. Soc.*, **2012**, *134*, 10071.
[13] J. Hou, H.-Y. Chen, S. Zhang, R. I. Chen, Y. Yang, Y. Wu, G. Li, *J. Am. Chem. Soc.* **2009**, *131*, 15586.
[14] M.-H. Chen, J. Hou, Z. Hong, G. Yang, S. Sista, L.-M. Chen, Y. Yang, *Adv. Mater.* **2009**, *21*, 4238.
[15] E. Wang, L. Hou, Z. Wang, S. Hellström, F. Zhang, O. Inganäs, M. R. Andersson, *Adv. Mater.* **2010**, *22*, 5240.
[16] T.-Y. Chu, J. Lu, S. Beaupr, Y. Zhang, J.-R. Pouliot, S. Wakim, J. Zhou, M. Leclerc, Z. Li, J. Ding, Y. Tao, *J. Am. Chem. Soc.* **2011**, *133*, 4250.

[17] H. Zhou, L. Yang, A. C. Stuart, S. C. Price, S. Liu, W. You, *Angew. Chem. Int. Ed.* **2011**, *50*, 2995.
[18] H.-Y. Chen, J. Hou, S. Zhang, Y. Liang, G. Yang, Y. Yang, L. Yu, Y. Wu, G. Li, *Nat. Photonics* **2009**, *3*, 649.
[19] C. Zhang, S. W. Tong, C. Jiang, E. T. Kang, D. S. H. Chan, C. Zhu, *Appl. Phys. Lett.* **2008**, *92*, 083310.
[20] S. Sista, Y. Yao, Y. Yang, M. L. Tang, Z. Bao, *Appl. Phys. Lett.* **2007**, *91*, 223508.
[21] J. Dai, X. Jiang, H. Wang, D. Yan, *Appl. Phys. Lett.* **2007**, *91*, 253503.
[22] J. Y. Kim, K. Lee, N. E. Coates, D. Moses, T.-Q. Nguyen, M. Dante, A. J. Heeger, *Science* **2007**, *317*, 222.
[23] J. Gilot, M. M. Wienk, R. A. J. Janssen, *Adv. Mater.* **2010**, *22*, E67.
[24] P. P. Khlyabich, B. Burkhart, B. C. Thompson, *J. Am. Chem. Soc.* **2011**, *133*, 14534.
[25] M. K. Siddiki, J. Li, D. Galipeau, Q. Qiao, *Energy Environ. Sci.* **2010**, *3*, 867.
[26] T. Ameri, G. Dennler, C. Lungenschmied, C. J. Brabec, *Energy Environ. Sci.* **2009**, *2*, 347.
[27] B. C. Thompson, P. P. Khlyabich, B. Burkhart, A. E. Aviles, A. Rudenko, G. V. Shultz, C. F. Ng, L. B. Mangubat, *Green* **2011**, *1*, 29.
[28] J.-H. Huang, M. Velusamy, K.-C. Ho, J.-T. Lin, C.-W. Chu, *J. Mater. Chem.* **2010**, *20*, 2820.
[29] B. C. Thompson, Y.-G. Kim, J. R. Reynolds, *Macromolecules* **2005**, *38*, 5359.
[30] M. Koppe, H.-J. Egelhaaf, G. Dennler, M. C. Scharber, C. J. Brabec, P. Schilinsky, C. N. Hoth, *Adv. Funct. Mater.* **2010**, *20*, 338.
[31] S. Honda, H. Ohkita, H. Bentena, S. Ito, *Chem. Commun.* **2010**, *46*, 6596.
[32] J. N. de Freitas, I. R. Grova, L. C. Akcelrud, E. Arici, N. S. Sariciftci, A. F. Nogueira, *J. Mater. Chem.* **2010**, *20*, 4845.
[33] L. Yang, H. Zhou, S. C. Price, W. You, *J. Am. Chem. Soc.* **2012**, *134*, 5432.
[34] P. P. Khlyabich, B. Burkhart, B. C. Thompson, *J. Am. Chem. Soc.* **2012**, *134*, 9074.
[35] C.-H. Chen, C.-H. Hsieh, M. Dubosc, Y.-J. Cheng, C.-S. Hsu, *Macromolecules* **2010**, *43*, 697.
[36] M. Campoy-Quiles, Y. Kanai, A. El-Basaty, H. Sakai, H. Murata, *Org. Electron.* **2009**, *10*, 1120.
[37] Y. Kim, M. Shin, H. Kim, Y. Ha, C.-S. Ha, *J. Phys. D: Appl. Phys.* **2008**, *41*, 225101.
[38] H. Kim, M. Shin, Y. Kim, *J. Phys. Chem. C* **2009**, *113*, 1620
[39] M. Koppe, H.-J. Egelhaaf, G. Dennler, M. C. Scharber, C. J. Brabec, P. Schilinsky, C. N. Hoth, *Adv. Funct. Mater.* **2010**, *20*, 338.
[40] A. A. Bakulin, D. Martyanov, D. Y. Paraschuk, P. H. M. van Loosdrecht, M. S. Pshenichnikov, *Chem. Phys. Lett.* **2009**, *482*, 99.
[41] W. J. Belcher, K. I. Wagner, P. C. Dastoor, *Sol. Energy Mater. Sol. Cells* **2007**, *91*, 447.
[42] J. H. Kwon, J.-Y. An, H. Jang, S. Choi, D. S. Chung, M.-J. Lee, H. Cha, J.-H. Park, C. E. Park, Y.-H. Kim, *J. Polym. Sci., Part A: Polym. Chem.* **2011**, *49*, 1119.
[43] S. Y. Bae, S. Y. Jo, K. H. Kim, T. W. Lee, D. H. Choi, *Mol. Cryst. Liq. Cryst.* **2011**, *538*, 175.
[44] J. Shin, N. S. Kang, K. H. Kim, T. W. Lee, J.-I. Jin, M. Kim, K. Lee, B. K. Ju, J.-M. Hong, D. H. Choi, *Chem. Commun.* **2012**, *48*, 8490.
[45] J. J. M. Halls, A. C. Arias, J. D. Mackenzie, W. Wu, M. Inbasekaran, E. P. Woo, R. H. Friend, *Adv. Mater.* **2000**, *12*, 498.
[46] V. I. Arkhipov, P. Heremans, H. Bässler, *Appl. Phys. Lett.* **2003**, *82*, 4605.
[47] V. I. Arkhipov, E. V. Emelianova, H. Bässler, *Phys. Rev. Lett.* **1999**, *82*, 1321.
[48] K. H. Jung, S. Y. Bae, K. H. Kim, M. J. Cho, K. Lee, Z. H. Kim, D. H. Choi, D. H. Lee, D. S. Chung, C. E. Park, *Chem. Commun.* **2009**, 5290.
[49] S. Y. Bae, K. H. Jung, M. H. Hoang, K. H. Kim, T. W. Lee, M. J. Cho, J.-I. Jin, D. H. Lee, D. S. Chung, C. E. Park, D. H. Choi, *Synth. Met.* **2010**, *160*, 1022.
[50] G. G. Malliaras, J. R. Salem, P. J. Brock, J. C. Scott, *J. Appl. Phys.* **1998**, *84*, 1583.
[51] M. D. Perez, C. Borek, S. R. Forrest, M. E. Thompson, *J. Am. Chem. Soc.* **2009**, *131*, 9281.
[52] V. D. Mihailetchi, P. W. M. Blom, J. C. Hummelen, M. T. Rispens, *J. Appl. Phys.* **2003**, *94*, 6849.